CMS Draft Analysis Note

The content of this note is intended for CMS internal use and distribution only

2010/07/02
Head Id: 9267
Archive Id: 6823:12523M
Archive Date: 2010/06/15
Archive Tag: trunk

Performance of variables used in jets + missing energy searches in 7 TeV data

R. Bainbridge[1], B. Betchart[2], H. Flächer[2], E. Laird[3], B. Mathias[1], T. Rommerskirchen[4], and M. Stoye[5]

[1] Imperial College, London, UK
[2] University of Rochester, Rochester, NY, USA
[3] Princeton University, Princeton, NJ, USA
[4] University of Zuerich, Zuerich, Switzerland
[5] CERN, Geneva, Switzerland

Abstract

We present studies of several jet based variables that are considered useful for discriminating against QCD background using the 2010 LHC collision data recorded at centre-of-mass energies of 7 TeV. The main focus is on quantities related to jets and missing energy in the events. In particular we investigate several angular variables involving jets, calorimetric missing energy and missing energy derived from jets (MHT) and compare the data distributions to the Monte Carlo expectation.

Contents

1 Introduction

We present a study of the 7 TeV data recorded with the CMS detector in the first half of 2010. We place particular focus on variables that are of interest for searches for supersymmetric (SUSY) signatures, specifically missing energy signatures. For these searches QCD multi-jet events where one of the jets has been mis-measured present a major background. We show first comparisons for data and Monte Carlo (MC) for variables that are powerful in rejecting QCD events. As in these events missing energy stems from mis-measurements rather than escaping, undetected particles, these studies address the performance of the CMS detector with regard to jets and missing energy. For our studies we compare three different types of jet reconstruction currently in use within CMS: purely calorimeter based jets (Calo jets), Jets-Plus-Tracks (JPT) jets that exploit the excellent performance of the CMS tracking detectors to improve the p_{T} response and resolution of calorimeter jets and Particle Flow (PF) jets which aim at identifying every particle in an event.

2 Analysis Code

The following describes the workflow and software used to derive at the results presented in this note. All the software used is available in cvs. From all RECO samples described in Section 3 so called Pat-Tuples have been created on the fly using the following recipe for the Physics Analysis Toolkit (PAT) in CMSSW_3_6_1:

```
cmsrel CMSSW_3_6_1
cd CMSSW_3_6_1/src
cmsenv
addpkg DataFormats/PatCandidates V05-09-15
addpkg PhysicsTools/PatAlgos V07-13-17
```

```
addpkg PhysicsTools/SelectorUtils V00-01-07
addpkg RecoMET/METAlgorithms V03-01-12
addpkg DataFormats/JetReco V03-28-04
addpkg PhysicsTools/PFCandProducer V04-05-04
cvs up -rV04-05-01-IsoDepVertexRelaxed PhysicsTools/PFCandProducer/python/Isolation/isoDeposits_c
addpkg RecoEgamma/EgammaTools V00-05-03
addpkg JetMETAnalysis/HcalReflagging V00-00-07
addpkg PhysicsTools/Configuration V00-07-02
cvs co -rV00-12-03 -dSUSYBSMAnalysis/SusyCAF UserCode/SusyCAF
scram b -j4
```

The recipe follows the SUSYPAT [1] definition from the SUSY group. In the same step flat nTuples have been generated from the on the fly created Pat-Tuples using the producers in UserCode/SusyCAF (V00-12-03).

`UserCode/SusyCAF/test/exampleTree_cfg.py.`

After this step all variables from PAT are accesible in the nTuple.

From the flat nTuple all plots are generated using

```
cvs co -r V01-03-08 -dSUSYBSMAnalysis/SusyCAFmacro UserCode/SusyCAFmacro
```

with the configuration

`UserCode/SusyCAFmacro/python/StandardPlots_cfg.py`

where all selection, as described later, are applied and all plots are produced.

3 Data and Monte Carlo Samples

The results presented in this note are based on the following data and MC samples:

- 7 TeV data:
  JetMETTau/Run2010A-May27thReReco_v1/RECO
  MinimumBias/Commissioning10-SD_JetMETTau-v9/RECO
  MinimumBias/Commissioning10-May6thPDSkim2_SD_JetMETTau-v1/RECO
  corresponding to the official JSON file from June 5th, 2010.
- 7 TeV PYTHIA QCD $\hat{p_T}$ >15:
  /QCD_Pt-15_7TeV-pythia8/Spring10-START3X_V26B-v1/GEN-SIM-RECO

4 Event and Object Selection

For the results presented in this note we follow the official recommendations for the 2010 Summer Conferences listed in [2]. In particular we follow the recommendations of the JetMET POG for jet selection and identification (JetID) listed in Refs. [3] and [4]. For details of the different types of jets considered in our analysis (Calorimeter Jets, Jets-Plus-Track, Particle Flow) we refer the reader to Ref. [3].

4.1 Trigger

We require the following triggers:

- L1 technical trigger bit 0 : consistent timing with LHC bunch crossing
- HLT single jet trigger HLT_Jet15U

Furthermore, we require the HLT PhysicsDeclared HLT bit which indicates that all CMS systems were operational with stable beams in the accelerator.

4.2 Vertex Requirement

We require at least one good vertex (! fake) with $N_{\mathrm{dof}} >= 5$ and vertex position along the beam direction of $|z_{\mathrm{vtx}}| < 15$ cm. Furthermore, we remove events with many fake tracks (also known as monster events) by requiring the ratio of HighPurity tracks over the total number of tracks to be greater than 25% in events that have 10 or more tracks.

4.3 Object Definitions

For the definition of jets we follow again the selection of the JetMET dijet analyses discussed in Ref. [3] and only briefly list the main selection criteria. For all three types of jet reconstruction (Calo, JPT, PF) we are using the anti-kt jet clustering algorithm [5] with jet cone size $R = 0.5$. For all three jet types, the leading jet is required to have energy-scale corrected $p_{\mathrm{T}} > 40\,\mathrm{GeV}$ and uncorrected $p_{\mathrm{T}} > 15\,\mathrm{GeV}$ to ensure a high-level trigger efficiency $> 95\%$ for the selected event samples. For the results presented in Section 5 we consider jets up to $|\eta| < 5$ while for those presented in Section 6 we only use jets up to $|\eta| < 3$. For the remaining jets in the event, the selection criteria are as follows:

- Calorimeter Jet definition:
  Jets are required to have corrected transverse momentum $p_{\mathrm{T}} > 20\,\mathrm{GeV}$ and to be within pseudo-rapidity $|\eta|$ <5. In order to reject noise from the calorimeters, jets are furthermore required to pass *loose* jet identification criteria (see Ref. [6]) that make

requirements on the minimum fraction of the jet energy contributed by electromagnetic calorimeter energy deposits (EMF), the number of RecHits contributing 90% of the jet energy (n90Hits), and the fraction of energy contributed by the highest hybrid photo-diode readout in the hadronic calorimeter (fHPD). Specifically, these are:

- ($|\eta| > 2.6$ OR $EMF > 0.01$)
- fHPD$<$0.98
- n90Hits$>$1

- Jets-Plus-Track Jet definition:
  Jets are required to have transverse momentum $p_{\mathrm{T}} > 20\,\mathrm{GeV}$ and to be within pseudo-rapidity $|\eta| <$5. Only jets within $|\eta| < 2$ receive a track-based energy and angular correction, due to the acceptance of the tracker. As JPT jets are corrected calo jets, the same "loose" jet identification criteria are applied as for calo jets.
- Particle Flow Jet definition:
  Particle Flow jets are requird to have transverse momentum $p_{\mathrm{T}} > 20\,\mathrm{GeV}$ and to be within pseudo-rapidity $|\eta| <$5. Similarly to Calo and JPT jets, jet identification criteria are also applied to PF jets, referred to as "loose extended" JetID (see Ref. [4]). Jets are required to have:
  - neutral hadron fraction < 1.0
  - neutral electromagnetic (photon) fraction < 1.0
  - charged electromagnetic (electron) fraction < 1.0
  - charged hadron fraction > 0.0 and charged multiplicity > 0.0 if $|\eta| < 2.4$

The jet identification cuts are mainly designed to reject noise from the Hadronic Calorimeter (HCAL).

4.4 Basic Jet Distributions

For the figures in this Section and Sec. 5 we require the two leading jets in the event to have transverse momentum $p_T > 40$ GeV, ensuring the used trigger HLT_Jet15U is > 90 % efficient for any of the three discussed jet reconstruction techniques.

To convince ourselves and the reader that the event and jet selection yields a reasonably clean sample of events with two or more jets we show some basic jet distributions. The Jet ID variables used for the selection of calorimeter jets are shown in Fig. 1 while the jet multiplicity distributions after the above event and object selection are shown in Fig. 2. In Fig. 3 the p_{T} spectra for the highest and second highest p_{T} jet in the events can be found.

In general the distributions are in good agreement with expectation and also the Monte Carlo simulation.

5 $\not\!\!E_T$ results at 7 TeV

In the following we show data - Monte Carlo comparisons for variables of interest to SUSY searches, in particular the SUSY Reference Analyses RA1 and RA2.

5.1 Missing Energy from Jets

Figure 4 shows the comparison of data to Monte Carlo simulated events for H_T, where the simulation is scaled to the number of events observed in data. The distributions shown in the left (a, c, and e) and right (b, d, and f) columns are for events that contain exactly two jets or

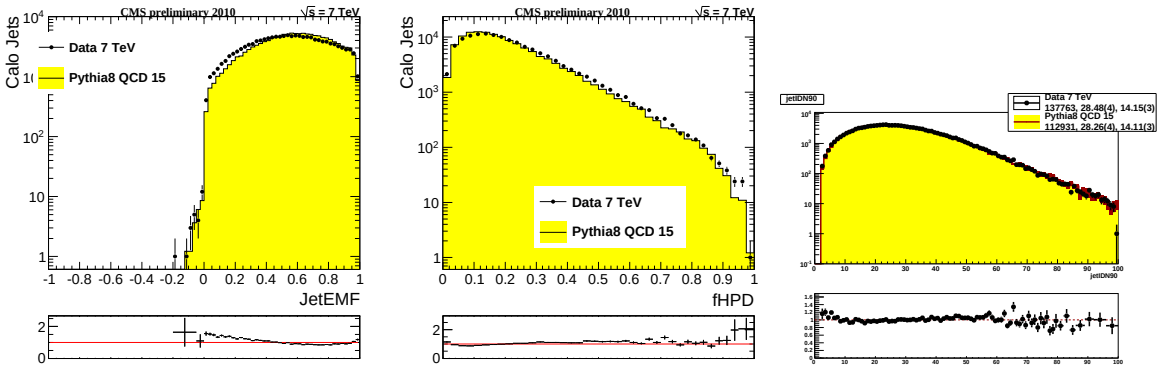

(a) f_{EM} (b) f_{HPD} (c) N_{90}

Figure 1: Variables used to determine the quality of the reconstructed jet and discriminate against noise. The distribution are shown for Calo jets as an example; from left to right: the fraction of the jet energy deposited in the ECAL (f_{EM}); the fraction of the jet energy read out by a single HPD in the HCAL (f_{HPD}); and the number of RecHits containing 90% of the shower signal (N_{90}).

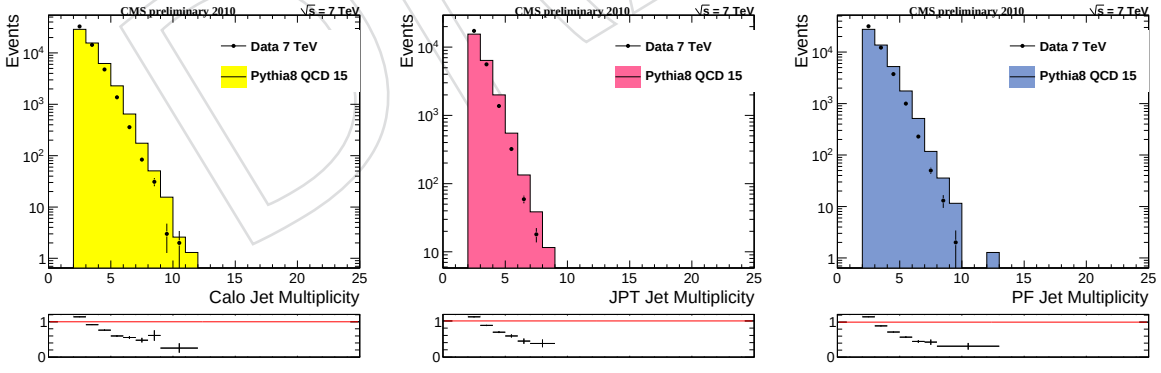

(a) (b) (c)

Figure 2: Jet multiplicity distributions after event and jet selection for Calo jets (left), JPT jets (centre) and Particle Flow jets (right).

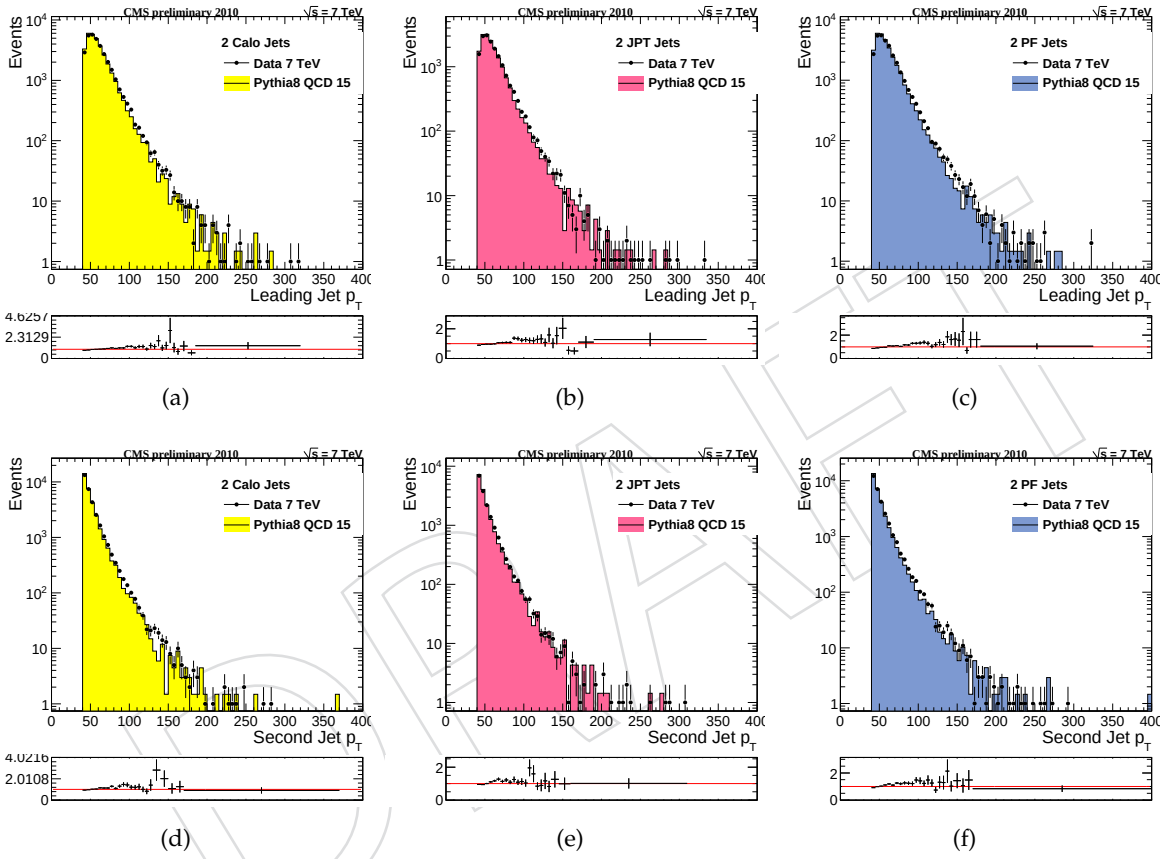

Figure 3: Corrected p_T distributions for the leading (top) and second leading (bottom) jet in events for various jet algorithms: Calo jets (left), JPT jets (centre) and Particle Flow jets (right).

three or more jets, respectively; the distributions in the top (a and b), middle (c and d) and bottom (e and f) rows are for calo jets, JPT jets and particle-flow jets, respectively. In each plot we show the expectation from a QCD PYTHIA 8 Monte Carlo simulation compared to data points (top window) and data divided by Monte Carlo to further examine the quality of the agreement in shape (bottom window). The data to Monte Carlo agreement is generally good. However, in the dijet case the data distribution is falling more slowly with H_T for all three types of jet reconstruction methods. In Fig. 5 we show the corresponding $\not{H}_T$ distributions for dijet events in the left column and three or more jets in the right column. The $\not{H}_T$ distributions for calo jets are displayed on top, for JPT jets in the middle and particle-flow jets at the bottom. No significant outliers are observed in any $\not{H}_T$ distribution. The small shoulder at $\sim 60\,\text{GeV}$ in the dijet distributions is a result of the applied jet p_T thresholds of 40 GeV on the leading jet and 20 GeV on all other jets. For a small fraction of events both jet p_T's are just above threshold and reconstructed in the same hemisphere while the balancing jets in the other hemisphere have fluctuated below the required jet p_T threshold.

To further evaluate the performance of the $\not{H}_T$ approach we study the dependence of the resolution of $\not{H}_T$ as a function of H_T. The resolution is obtained as the σ of a Gaussian fit to the $\not{H}_{x,y}$ distributions. In Fig. 6 we compare the resolutions of $\not{H}_T$ for events with exactly two jets and three or more jets in data and Monte Carlo. For comparison, we also plot the corresponding $\not{E}_T$ resolutions. It can be seen that $\not{H}_T$ has a slightly worse resolution than $\not{E}_T$, due to the fact that $\not{H}_T$ does not take into the account the unclustered energy in each event. The effect is more pronounced when comparing to pf$\not{E}_T$, which uses a more sophisticated $\not{E}_T$ reconstruction method.

We also assess the size of the tails in the $\not{H}_T$ and $\not{E}_T$ distributions, *i.e.*, deviations from Gaussian behaviour. A good understanding of these tails is of particular importance for searches of new physics involving weakly interacting particles that escape the detector. To first approximation, disregarding detector noise, beam-halo events, pile-up and similar effects, $\not{E}_{x,y}$ ($\not{H}_{x,y}$) is expected to be Gaussian with a σ that depends on $\sum E_\text{T}$ (H_T). We test this through the following procedure. To eliminate the dependence of the missing energy on the total energy in the event we devide $\not{E}_{x,y}$ by $\sqrt{\sum E_\text{T}}$ and $\not{H}_{x,y}$ by $\sqrt{H_T}$. We then determine the core width σ_{fit} of the $\not{E}_{x,y}/\sqrt{\sum E_\text{T}}$ and $\not{H}_{x,y}/\sqrt{H_T}$ distributions by iteratively fitting a Gaussian distribution to the events contained within $\pm 1.5\sigma$. In the case of perfect Gaussian behaviour, 68.3% of the events are contained within $\pm 1\sigma_{fit}$. We then find the actual range containing 68.3% of events in the observed distribution. Because of the non-Gaussian tails in the distribution this range deviates from σ_{fit} by some factor θ_1. This procedure defines a point $(1, \theta_1)$ in Fig. 7. We then repeat this procedure for different multiples of σ, finding the actual $\not{H}_{x,y}/\sqrt{H_T}$ range, $\pm\theta_n$, expressed as a multiple of σ_{fit}, that contains the corresponding fraction of events. We then plot θ_n versus n in Fig. 7. More rigorously θ_n can be defined as

$$\theta_n = F^{-1}(G(n))/\sigma_{fit} \tag{1}$$

where $G(n)$ is the cumulative distribution for a half-normal Gaussian with unit σ and F is the cumulative distribution of $|\not{H}_{x,y}|$. The solid line in Fig. 7 represents the diagonal $\theta_n = n$, which corresponds to the perfect Gaussian behaviour. It is clear that above 2-2.5 σ the distributions start deviating from the Gaussian behaviour. The agreement between data and Monte Carlo is very good for both $\not{E}_T$ and $\not{H}_T$ cases, with the tails in data being only slightly larger in the case of calo jets. For calo jets, the tail in the calo$\not{E}_T$ distribution is somewhat smaller than in the corresponding $\not{H}_T$ distribution, while particle-flow jets, the $\not{H}_T$ and pf$\not{E}_T$ tails agree very well up to $n \sim 3.5$. In general, it is very encouraging to see that also the non-Gaussian tails in the $\not{E}_T$ and $\not{H}_T$ distributions are modelled well by the simulation.

6 SUSY results at 7 TeV

6.1 Event Selection

In addition to the event selection described in Section 5, we only use jets up to $|\eta| < 3$ in the following. While the dijet analysis of Ref. [3] requires the azimuthal angle between the two jets to be $> \pi - 1$ rad, we do not apply such a cut as it is undesirable for a SUSY event selection. Even though the majority of our selected events has exactly two jets, we do allow for extra jets in the event.However, to further protect against noise from the calorimeters we reject events with jet candidates that pass the jet p_{T} threshold but fail the $|\eta| < 3$ requirement or the Jet ID criteria. With this we make sure that no identified high p_{T} object is present in the event that otherwise could lead to missing energy in the event. This last requirement rejects approximately 7% of events in the case of Calo Jets, $\sim$ 9% of events for JPT jets, and $\sim$ 4% of events in the case of PF jets.

6.2 Alternative Variables

In this section two alternative selection variables are discussed. These variables are $\Delta\phi^*$ a variables mainly based on the angular distance of jets in an event, and α_T which exploits both the angular distance and the relative momentum of jets.

$\Delta\phi^*$: In SM events without neutrinos large missing energy is in most cases due to severe mis-measurement of at least one of the leading jets. This fact is exploited by the variable $\Delta\phi^*$, which is the minimal azimuthal distance between a jet and *biased* H_T^{miss}, where *biased* H_T^{miss} is calculated from all selected jets, but the jet under test. The formula for $\Delta\phi^*$ is:

$$\Delta\phi^* = \min_k(\Delta\phi((\sum_{j=0}^{j=n} -\vec{j}_i) + \vec{j}_k, \vec{j}_k)), \tag{2}$$

where n is the number of jets and $\vec{j}_i$ the momentum of jets. This variable tests if there is at least one jet which, if rescaled by a certain factor, would be able to balance the event. For typical QCD events, with one dominating jet mis-measurement, this angle tends to be small. Both for under and for over estimated jet energies the tested jet and the *biased* H_T^{miss} should point into the same ϕ-direction. The distribution of $\Delta\phi^*$ is shown in Fig. 8, for calorimeter, JPT, and Particle Flow jets. Independent of the jet definition the $\Delta\phi^*$ distribution MC predictions tend to overestimate the number of events at large values of $\Delta\phi^*$. However, tests with different tunes of PYTHIA showed that there is a sensitivity to the tuning of PYTHIA to some extend.

α_T**:** The variable α was first suggested by L. Randall et al. [7] to exploit the typical topology of two back-to-back jets of equal magnitude in dijet QCD events. The definition of α in dijet events is:

$$\alpha = E_T(j_2)/M_{inv.}, \tag{3}$$

where $E_T(j2)$ is the transverse energy of the jet with the lowest transverse momentum and M_{inv} is the invariant mass of the two jets. In Ref. [8] a modified version of α is explored (α_T) in which the transverse mass $M_{T,inv}$ of the two jets (j):

$$M_{T,inv} = \sqrt{\left[\sum_{i=1}^{2} E_T(j_i)\right]^2 - \left(\sum_{i=1}^{2} \vec{p}_t(j_i)\right)^2} \tag{4}$$

is used instead of the invariant mass.

The extension of α_T to searches with more than two jets is discussed in Ref. [9]. To define α_{T} in events with at least two jets a system of n-jets is reduced to a two-jet system by combining jets into two pseudo-jets. The transverse momentum of the pseudo-jets p_T^{pj} is calculated as the scalar sum of the contributing jets. All combinations of jets are computed and the one is chosen for which the difference $\Delta H_{\mathrm{T}} = p_T^{pj_1} - p_T^{pj_2}$ is minimal. The variable α_{T} is then defined as:

$$\alpha_{\mathrm{T}} = \frac{1}{2}\frac{H_{\mathrm{T}} - \Delta H_{\mathrm{T}}}{\sqrt{H_{\mathrm{T}}^2 - (H_{\mathrm{T}}^{\mathrm{miss}})^2}} = \frac{1}{2}\frac{1 - \Delta H_{\mathrm{T}}/H_{\mathrm{T}}}{\sqrt{1 - (H_{\mathrm{T}}^{\mathrm{miss}}/H_{\mathrm{T}})^2}}. \tag{5}$$

For two jets this evaluates to:

$$\alpha_{\mathrm{T}} = \frac{p_T(j_2)}{\sqrt{\left(\sum_{i=1}^{2} p_T(j_i)\right)^2 - \left(\sum_{i=1}^{2} \vec{p}_t(j_i)\right)^2}}, \tag{6}$$

which is equal to the α_T definition in Ref. [8] for massless jets. The distribution of α_T is shown in Fig. 9 for a 7 TeV Monte Carlo study with the same selection described in Ref. [9] ($H_T > 350$ GeV, jets > 50 GeV). α_T of the real data (no H_T cut and jets > 20 GeV) are shown in Fig. 10, for calorimeter jets, JPT jets and Particle Flow jets. Both data and MC agree reasonably well, in the dijet and multijet case and for all jet types.

Both variables $\Delta\phi^*$ and α_T don't depend directly on the jet-energy scale. For this kind of variables the resolution improves with increasing H_T [9]. This is visible in Fig. 11,12,13,14 which show the variable distributions for different bins of H_T. For $\Delta\phi^*$ the distribution get more narrow with increasing H_T cuts and for α_T the tail of the distribution gets reduced with increasing H_T values.

An interesting application of this behavior is discussed in Ref. [9] for α_T as final selection variable. The application is based on a combination of three different variables, $|\eta|$ of the leading jet, H_T and the fraction f:

$$f = \frac{\#\text{ events } \alpha_T > 0.55}{\#\text{ all events}}. \tag{7}$$

Due to the high mass of SUSY particle the presence of a SUSY signal is expected to manifest itself with two distinctive features [9]:

- tighter requirements on H_{T} increase f,
- the increase in f is largest at small values of $|\eta|$.

Whereas if no SUSY signal is present f is expected to decrease for QCD events with increasing H_T. As presented in Fig. 15 for α_T and a cut at 0.55 and in Fig. 16 for a selection on $\Delta\phi^* > 0.8$ the measured fraction f decreases as expected with H_T. Data and MC prediction are either similar or, if any deviation, the MC predicts more selected events than observed in data. The only exception is visible in Fig. 15 f), in this case the fraction is zero for MC but not for data as in data one event passes the requirement of $\alpha_T > 0.55$ and $H_T > 160$ GeV/c. The upper limit for the mean of a Poisson variable for confidence levels of 68% and 0 selected MC events is about 3. Taking this into account one can conclude that also this excess is not significant.
Further it is also tested if the fraction f is constant with $|\eta|$ of the leading jet, as it is expected for QCD. Fig. 17 shows the fraction f as a function of $|\eta|$ of the leading jet and with an H_T

threshold of 160 GeV. Data and MC agrees reasonably well. As a further test one out of 25 jets was randomly removed to mimic extreme mismeasurements. Also for this modified data the fraction f remains flat and is hence distinct from typical SUSY signal, which is more central [9].

Another interesting test is the comparison of the measured $\Delta\phi^*$ to a modeling of the expected Signal of SUSY events in which LSP escape from the detector. This modeling has been performed by deleting in data by random choice on of the jets in every event. The resulting distribution is shown in Fig. 18 together with the measured $\Delta\phi^*$ distribution, once for dijet events and once for events with more than two jets, for calorimeter and for PF jets. Fig. 19 shows how the $\Delta\phi^*$ distribution evolves with H_T for both, with and without deleted jet.

7 Conclusion

We carried out a first analysis of the 7 TeV LHC data recored by CMS in 2010. We placed focus on variables that useful for QCD background rejection in SUSY searches with missing energy. For this, we studied events with two or more jets. Amongst other observables we studied the correlation between unclustered energy in the calorimeters and clustered, jet based observables. We compared the performance of three different types of jet reconstruction, Calo jets, JPT jets and PF jets, and generally observe a good agreement between data and simulation.

References

[1] https://twiki.cern.ch/twiki/bin/view/CMS/SusyPatLayer1DefV7.

[2] https://twiki.cern.ch/twiki/bin/viewauth/CMS/METichepPAS2.

[3] Jet Commissioning using Di-Jet Events from 900 GeV and 2360 GeV Collision Data, CMS AN-2010/009.

[4] Particle Flow Jet Identification Criteria, CMS AN-2010/003.

[5] M. Cacciari, G. P. Salam, and G. Soyez, "The anti-kt jet clustering algorithm", *JHEP* **0804:063** (2008).

[6] Calorimeter Jet Quality Criteria for the First CMS Collision Data, and preparations for calibrating their efficiencies, CMS AN-2009/087.

[7] L. Randall and D. Tucker-Smith, "Dijet Searches for Supersymmetry at the LHC", *Phys.Rev.Lett.* **101 221803** (2008).

[8] C. Collaboration, "SUSY searches with dijet events", *CMS PAS* **SUS-08-005** (2008).

[9] C. Collaboration, "Search for SUSY with exclusive hadronic N-Jet Events", *CMS PAS* **SUS-09-001** (2009).

8 Appendix

This appendix contains plots organized in the following fashion:

- Clustered energy (H_{T}, $\not{H}_T$, $\not{H}_T$ core resolution, $\not{H}_T$ tail shape)
- Compare $\not{H}_T$,$\not{E}_T$ (resolution, tail shape)
- Other variables for SUSY searches (minimum $\Delta\phi_{\mathrm{biased}}$, α_T)

8.1 Clustered Energy

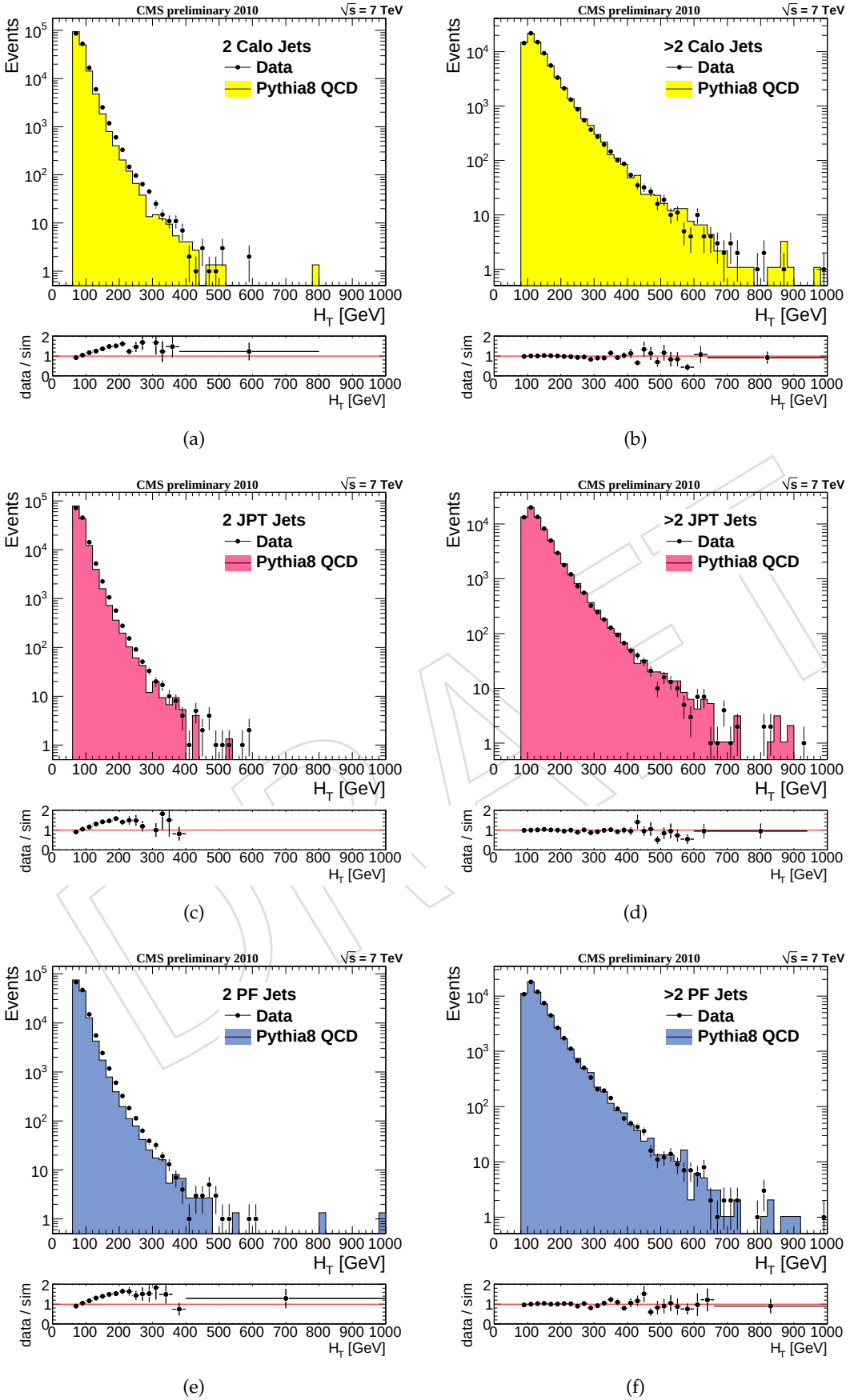

Figure 4: H_T distributions for calorimeter jets (left), JPT jets (middle) and PF jets (right). Distributions for dijet events are shown in the top row, for >= 3 jets in the bottom row.

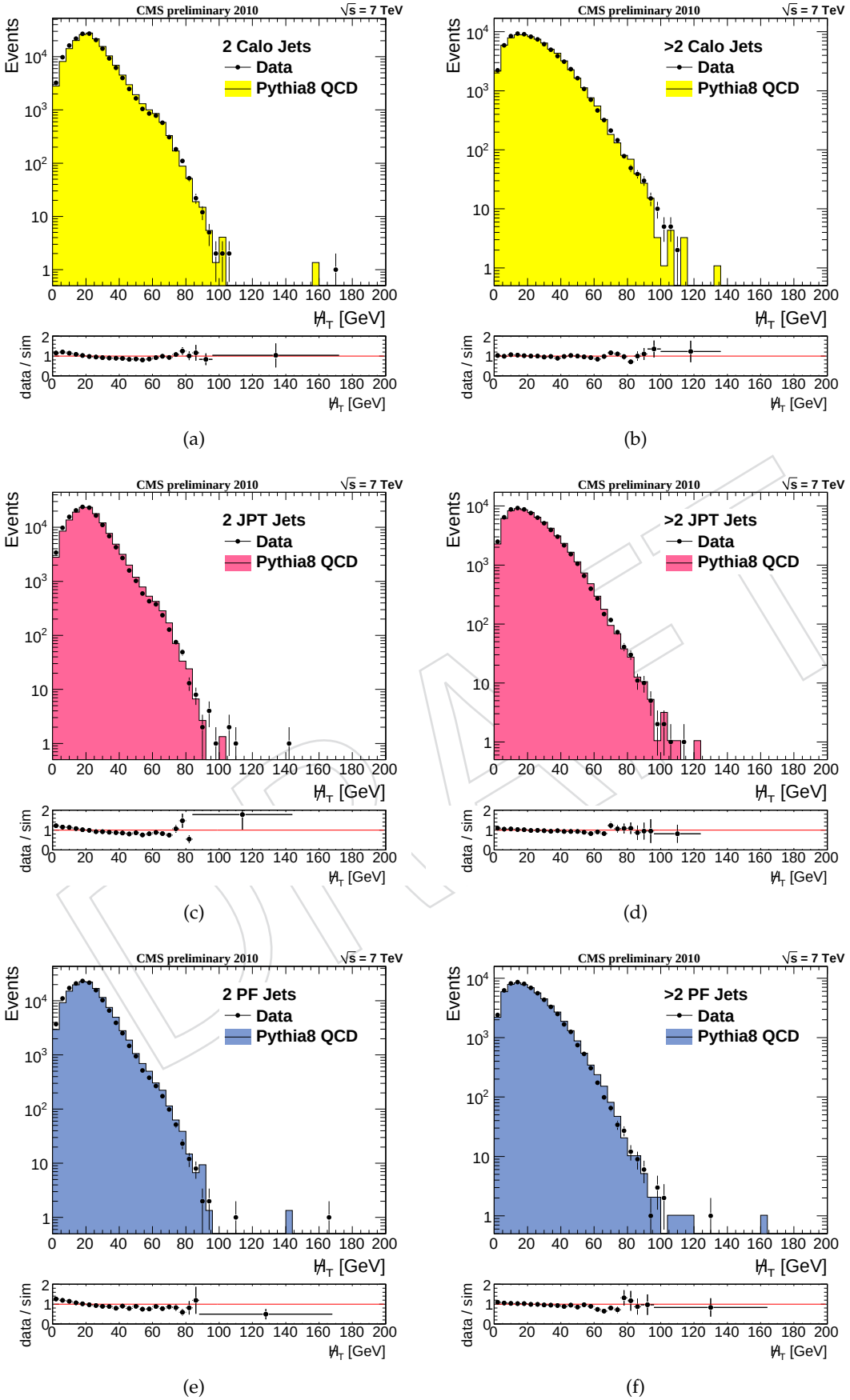

Figure 5: $\not\!\!H_T$ distributions for calorimeter jets (left), JPT jets (middle) and PF jets (right). Distributions for dijet events are shown in the top row, for >= 3 jets in the bottom row.

h!

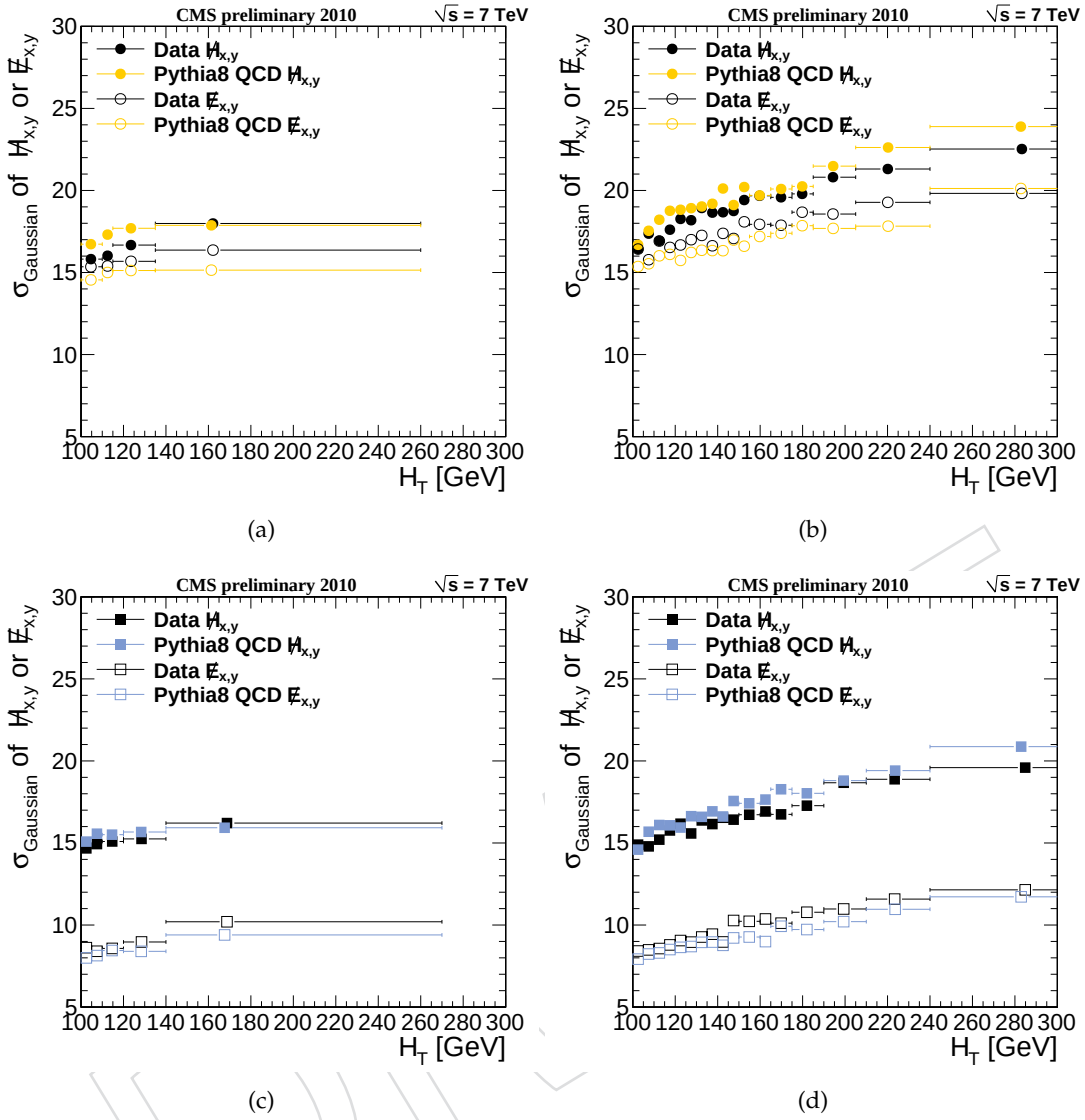

Figure 6: Comparison of MHT and MET resolutions as a function of HT for dijet events (left column) and events with $>= 3$ jets (right column). The MHT and MET resolutions for calorimeter jets are show in the top row, for PF jets in the bottom row.

8.2 Comparisons between clustered and unclustered energy

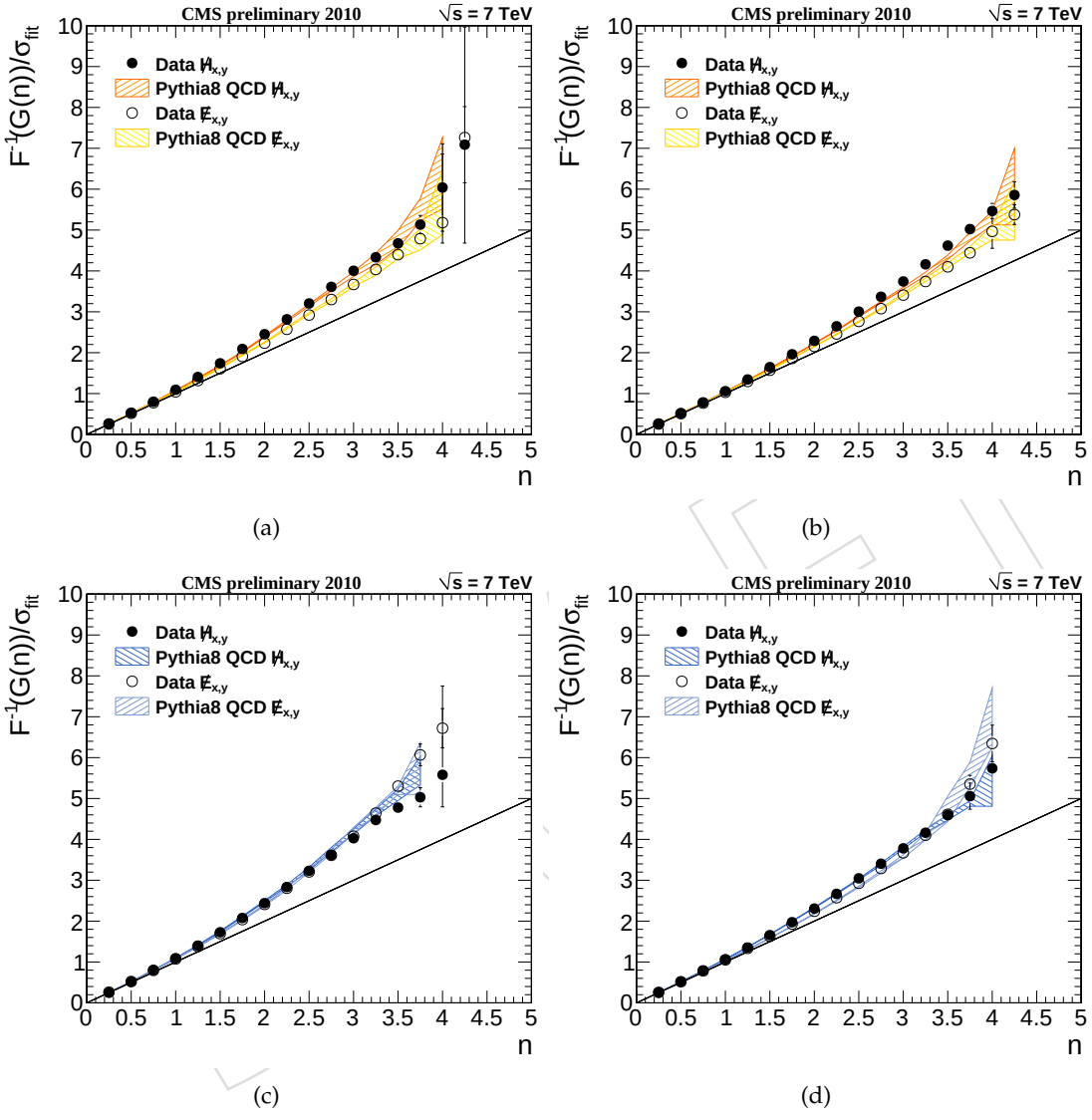

Figure 7: Comparison of Gaussian behavoir of MHT and MET tails for dijet events (left) and events with $>= 3$ jets (right). Deviation from Gaussian behaviour for MHT from calorimeter jets is shown in the top plots, for MHT from PF jets in the bottom plots.

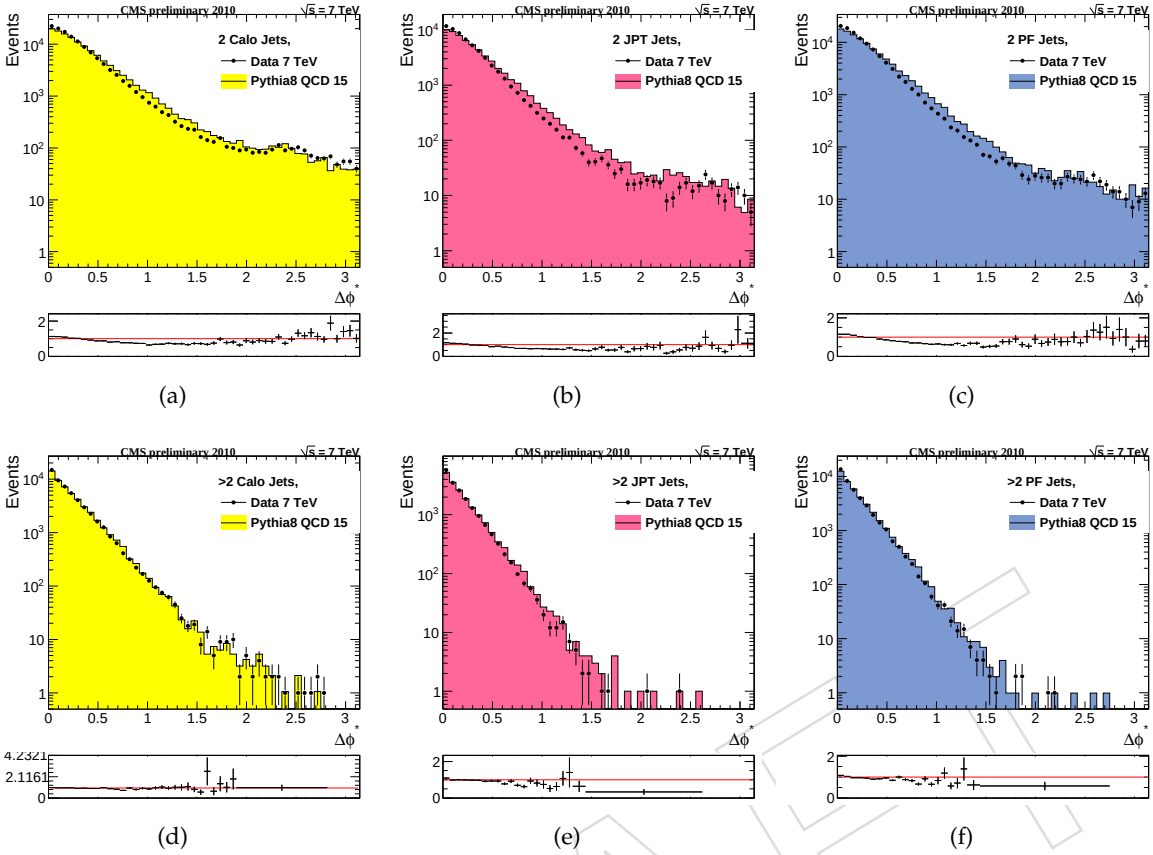

Figure 8: $\Delta\phi^*$ distributions for Calorimeter, JPT, and PF jets (left to right) in dijet (top) and multijet (bottom) events.

8.3 Susy Distributions

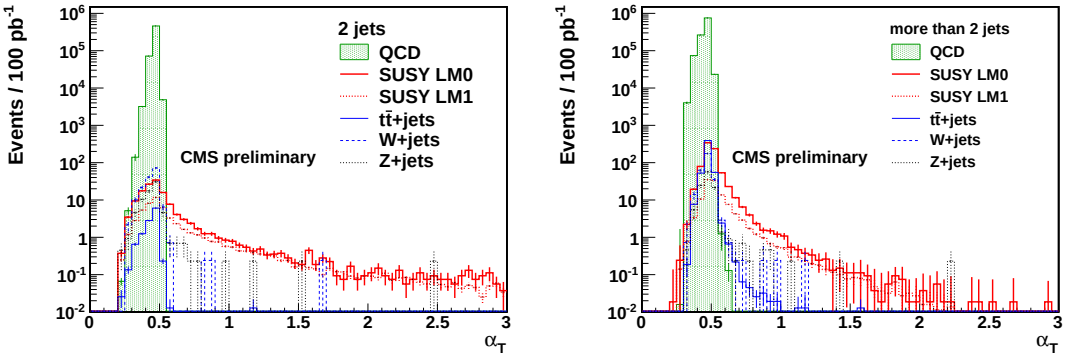

(a) (b)

Figure 9: Simulated α_T distributions for dijet (left) and multijet (right) events. Selection as in Ref [9]

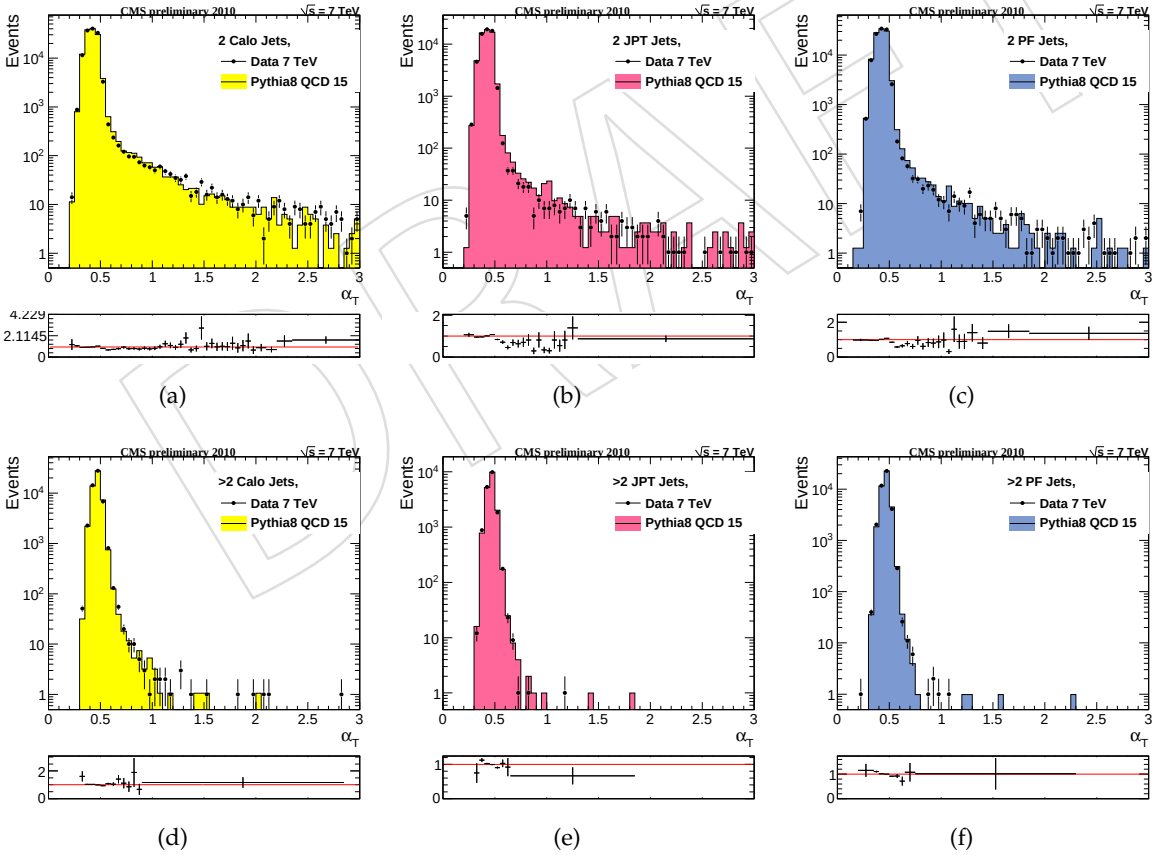

(a) (b) (c)

(d) (e) (f)

Figure 10: α_T for Calorimeter, JPT, and PF jets (left to right), for dijet (top) and multijet (bottom) events.

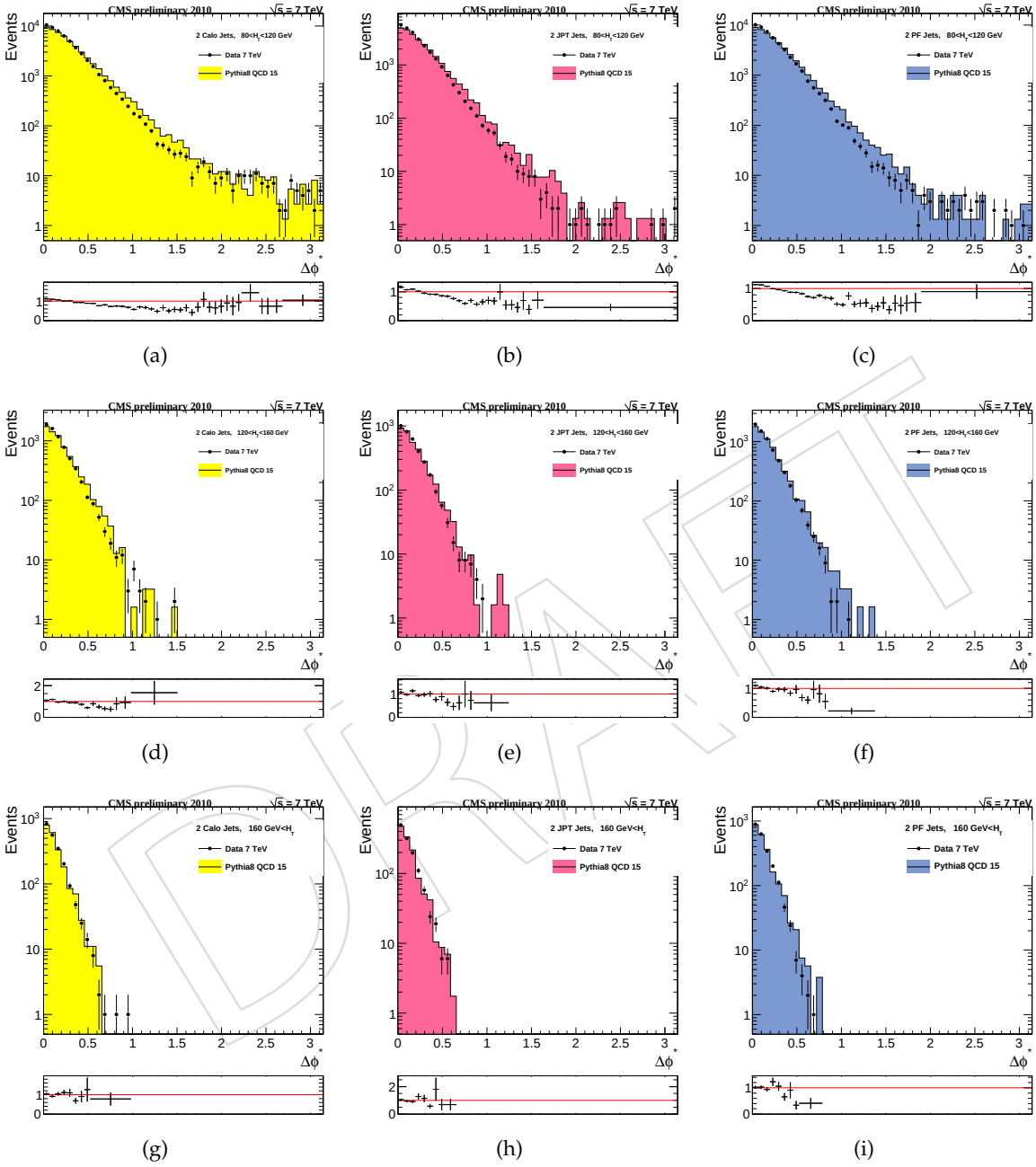

Figure 11: $\Delta\phi^*$ in dijet events, shown for Calorimeter, JPT, and PF jets (left to right) for events of increasing H_T range (top to bottom). The H_T ranges in GeV are [80,120],[120,160],[160,].

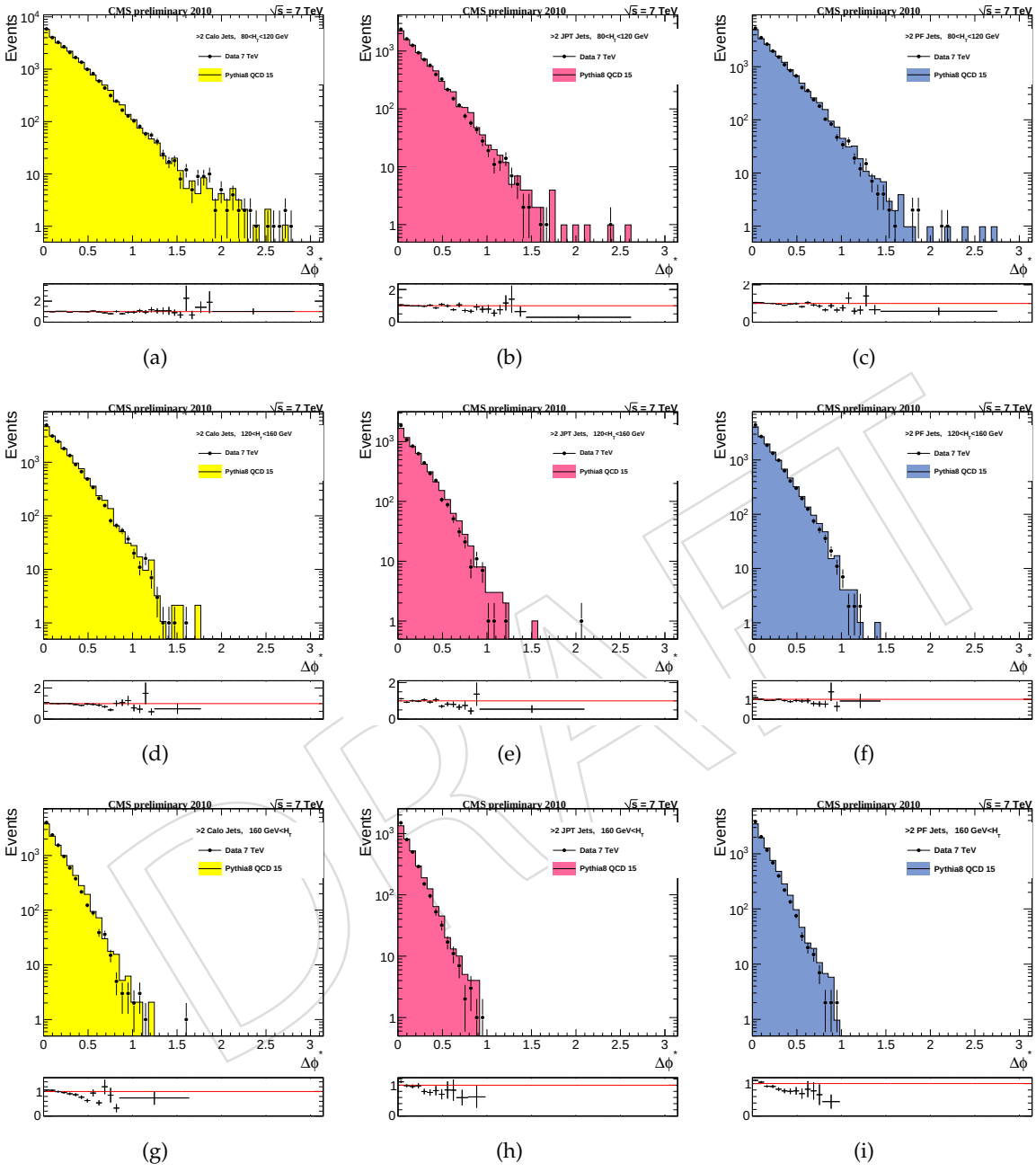

Figure 12: $\Delta\phi^*$ in multijet events, shown for Calorimeter, JPT, and PF jets (left to right) for events of increasing H_T range (top to bottom). The H_T ranges in GeV are [80,120],[120,160],[160,].

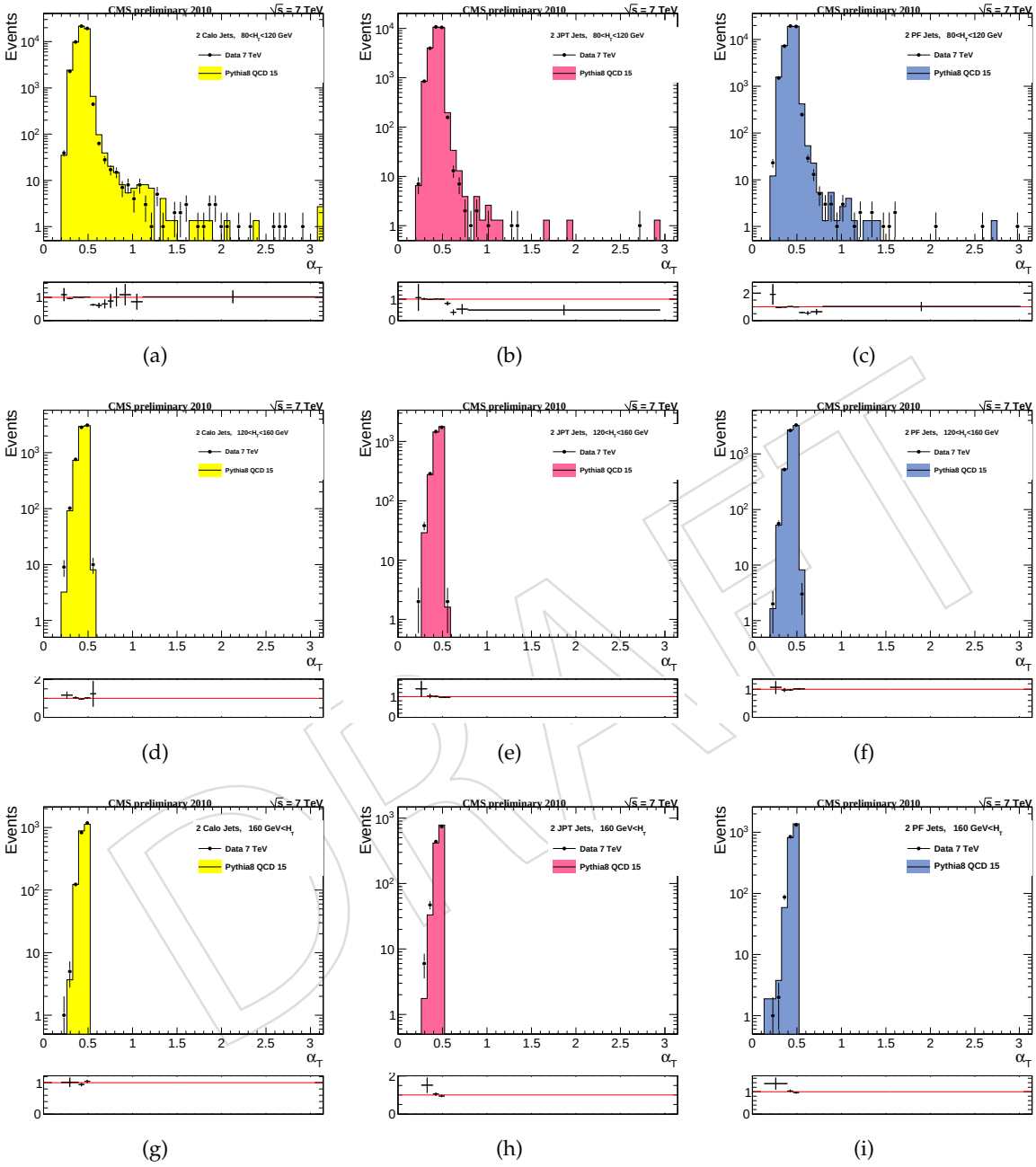

Figure 13: α_T in dijet events, shown for Calorimeter, JPT, and PF jets (left to right) for events of increasing H_T range (top to bottom). The H_T ranges in GeV are [80,120],[120,160],[160,].

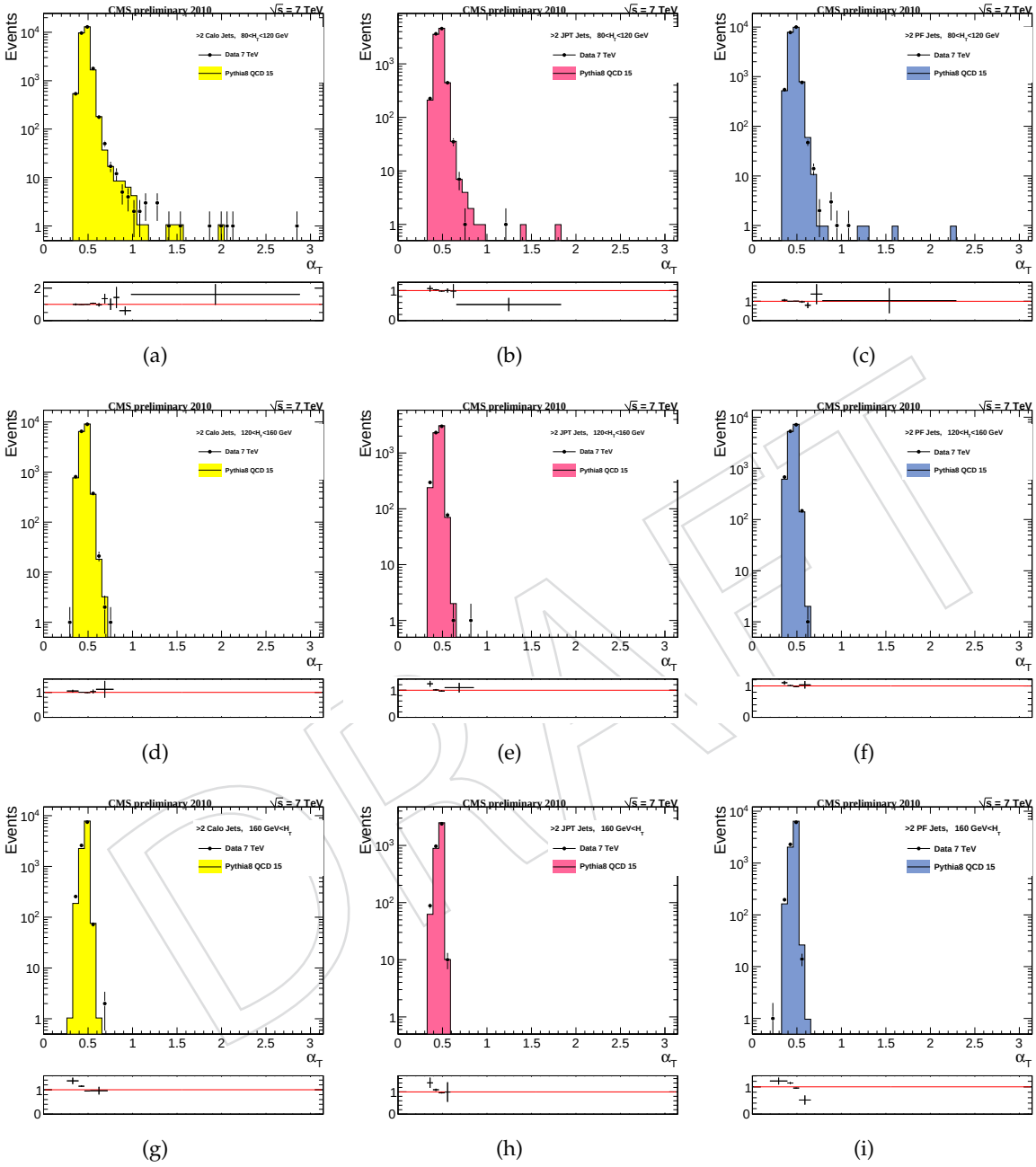

Figure 14: α_T in multijet events, shown for Calorimeter, JPT, and PF jets (left to right) for events of increasing H_T range (top to bottom). The H_T ranges in GeV are [80,120],[120,160],[160,].

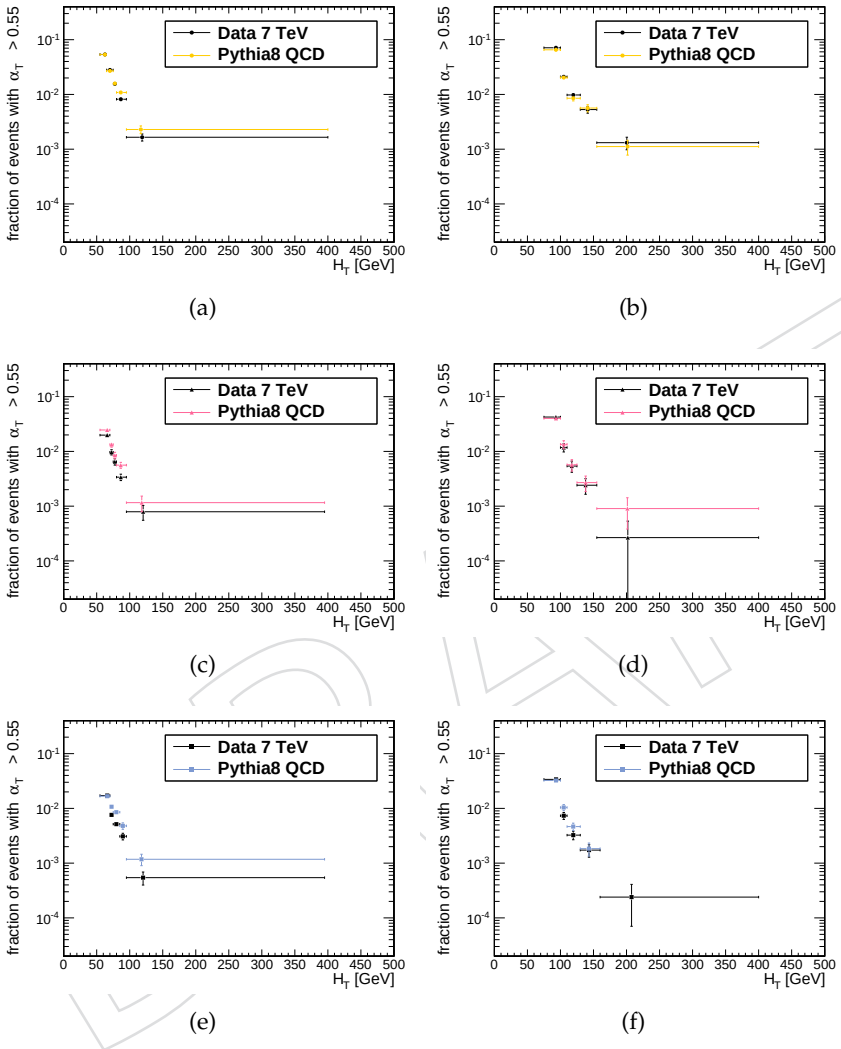

Figure 15: Fraction f of events with $\alpha_T > 0.55$ vs H_T. The plots on the left are for dijet events, the plots on the right for events with more than two jets. The first row from the top shows the distribution for calorimeter jets, the second row for JPT jets, and the third for PF jets.

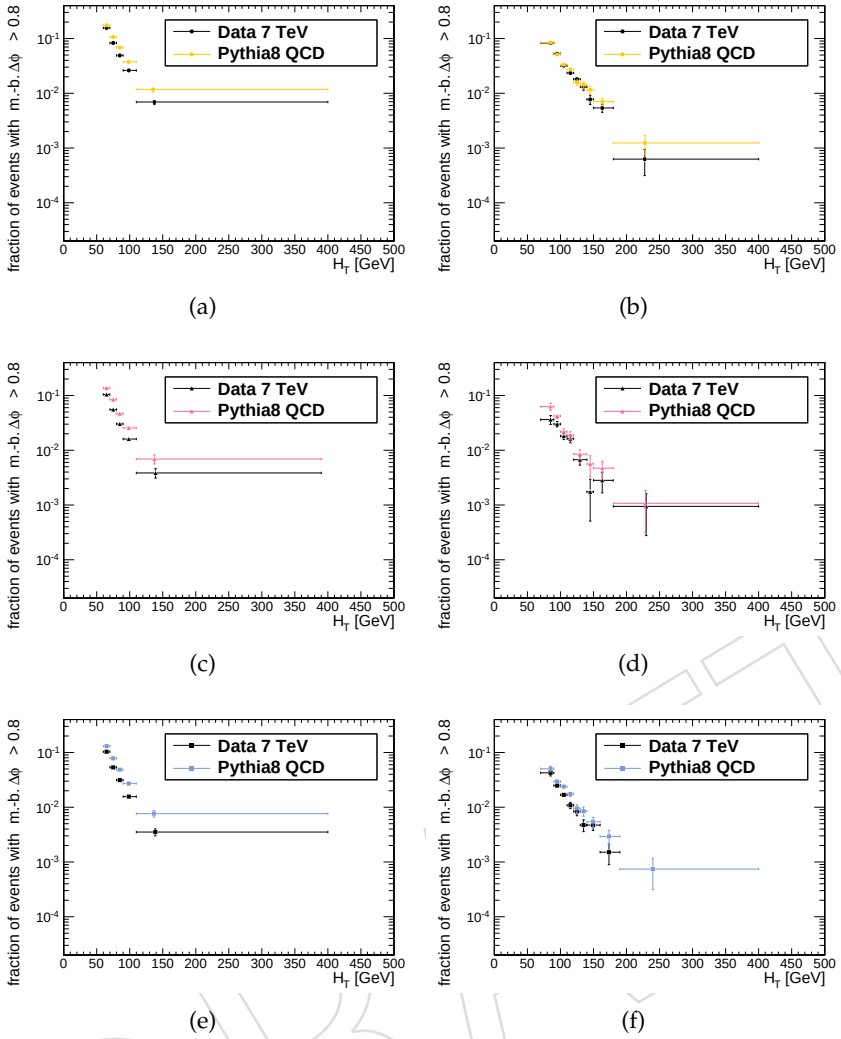

Figure 16: Fraction f of events with $\Delta\phi^* > 0.8$ vs H_{T}. The plots on the left are for dijet events, the plots on the right for events with more than two jets. The first row from the top shows the distribution for calorimeter jets, the second row for JPT jets, and the third for PF jets.

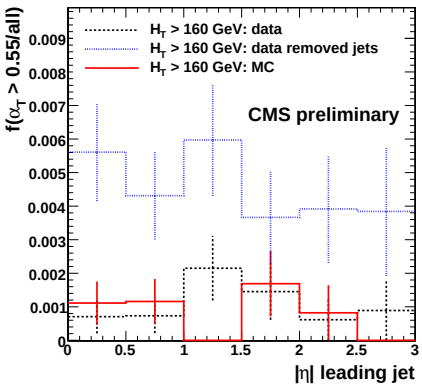

Figure 17: The fraction f as a function of $|\eta|$ leading jet for events with $H_T > 160$ GeV for data, data with one out of 25 jets deleted, and MC.

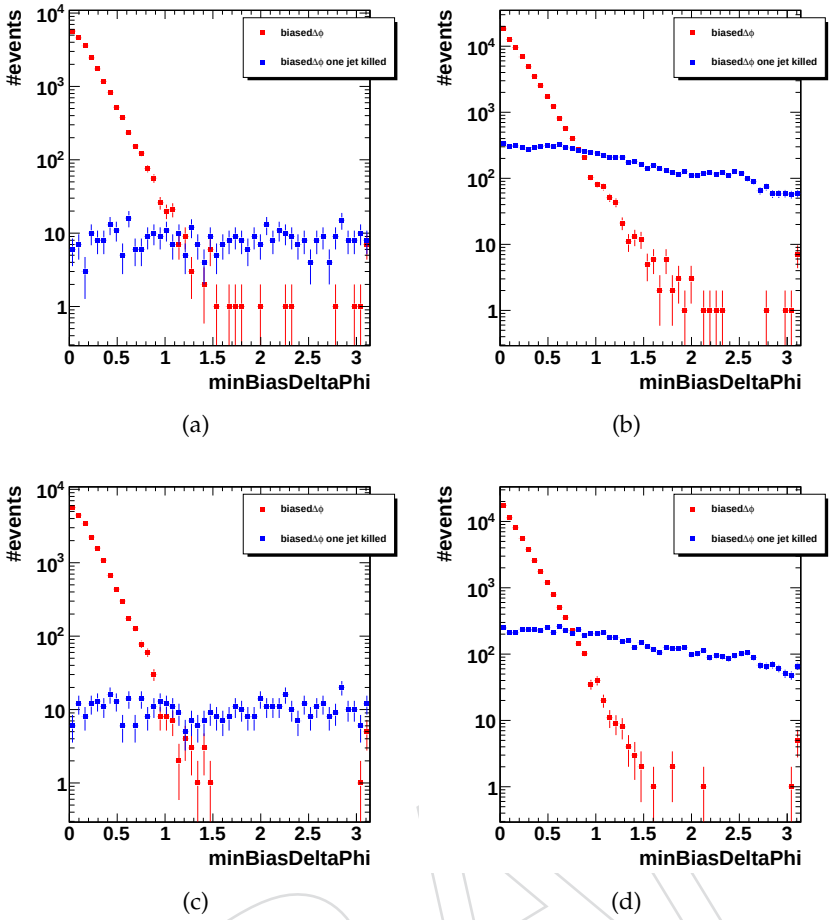

Figure 18: The $\Delta\phi^*$ distribution together with $\Delta\phi^*$ distribution in events in which one jet has been deleted. The plots on the left are for dijet events, the plots on the right for events with more than two jets. The first row from the top shows the distribution for calorimeter jets and the second row for PF jets.

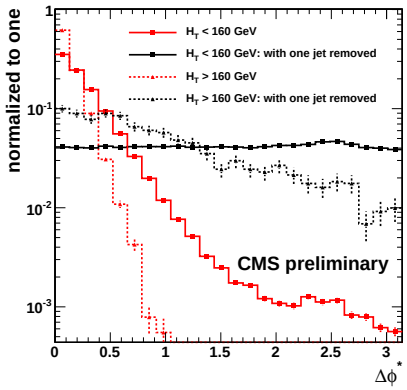

Figure 19: The $\Delta\phi^*$ distribution together with $\Delta\phi^*$ distribution in events in which one jet has been deleted for calorimeter jets and for different H_T ranges.